Optical Imaging of Cancer Heterogeneity with Multispectral Optoacoustic Tomography[1]

Eva Herzog, PhD
Adrian Taruttis, MS
Nicolas Beziere, PhD
Andrey A. Lutich, PhD
Daniel Razansky, PhD
Vasilis Ntziachristos, PhD

Purpose: To investigate whether multispectral optoacoustic tomography (MSOT) can reveal the heterogeneous distributions of exogenous agents of interest and vascular characteristics through tumors of several millimeters in diameter in vivo.

Materials and Methods: Procedures involving animals were approved by the government of Upper Bavaria. Imaging of subcutaneous tumors in mice was performed by using an experimental MSOT setup that produces transverse images at 10 frames per second with an in-plane resolution of approximately 150 μm. To study dynamic contrast enhancement, three mice with 4T1 tumors were imaged before and immediately, 20 minutes, 4 hours, and 24 hours after systemic injection of indocyanine green (ICG). Epifluorescence imaging was used for comparison. MSOT of a targeted fluorescent agent (6 hours after injection) and hemoglobin oxygenation was performed simultaneously (4T1 tumors: $n = 3$). Epifluorescence of cryosections served as validation. The accumulation owing to enhanced permeability and retention in tumors (4T1 tumors: $n = 4$, HT29 tumors: $n = 3$, A2780 tumors: $n = 2$) was evaluated with use of long-circulating gold nanorods (before and immediately, 1 hour, 5 hours, and 24 hours after injection). Dark-field microscopy was used for validation.

Results: Dynamic contrast enhancement with ICG was possible. MSOT, in contrast to epifluorescence imaging, showed a heterogeneous intratumoral agent distribution. Simultaneous imaging of a targeted fluorescent agent and oxy- and deoxyhemoglobin gave functional information about tumor vasculature in addition to the related agent uptake. The accumulation of gold nanorods in tumors seen at MSOT over time also showed heterogeneous uptake.

Conclusion: MSOT enables live high-spatial-resolution observations through tumors, producing images of distributions of fluorochromes and nanoparticles as well as tumor vasculature.

Supplemental material: *http://radiology.rsna.org/lookup/suppl/doi:10.1148/radiol.11111646/-/DC1*

[1] From the Institute for Biological and Medical Imaging, Technische Universität München and Helmholtz Zentrum München, Ingolstädter Landstrasse 1, 85764 Neuherberg, Germany (E.H., A.T., N.B., D.R., V.N.); and Photonics and Optoelectronics Group, Department of Physics and CeNS, Ludwig-Maximilians-Universität München, Munich, Germany (A.A.L.). Received August 5, 2011; revision requested September 26; revision received November 17; accepted December 8; final version accepted December 9. A.A.L. supported by Nanosystems Initiative Munich. D.R. supported by a DFG Research Grant (grant RA 1848/1) and ERC Starting Grant. V.N. supported by an ERC Senior Investigator Award and Medizin Technik BMBF Award. **Address correspondence to** V.N. (e-mail: *v.ntziachristos@tum.de*).

Fluorescence intravital microscopy is essential for understanding the cancer microenvironment and treatment mechanisms (1,2). Such imaging of tumors has allowed substantial insights into tumor vasculature and the micropharmacokinetic properties of therapeutics by means of fluorescence. Despite the important benefits of fluorescence microscopy, it suffers from superficial penetration: Imaging depths rarely reach beyond a few hundred micrometers (3). Macroscopic imaging of entire tumors could reveal the spatial heterogeneity not captured with microscopy, for example, the overall distribution of drug delivery. However, optical macroscopic methods are limited by photon diffusion and are today mainly applied as qualitative two-dimensional approaches that capture fluorescence photons that reach the skin surface, concealing information about intratumoral biodistribution (3). The emergence of optoacoustic imaging brings a new ability to study tumors by providing high-spatial-resolution deep-tissue optical contrast and real-time operation (4–6).

Optoacoustic imaging illuminates the tissue with short photon pulses (nanosecond range) and depicts ultrasonic waves generated in response to the absorption of light by the various tissue absorbers (7). By applying multiple-wavelength illumination, multispectral optoacoustic tomography (MSOT) in particular (8,9) can help differentiate common fluorochromes, light-absorbing nanoparticles, or hemoglobin by their spectral signatures, potentially offering the advantages of fluorescence microscopy, with penetration depths of several millimeters up to centimeters of tissue, at resolutions limited by the scattering of ultrasound waves—which is orders of magnitude less than that of light (3).

To date, imaging based on the optoacoustic phenomenon has been applied in a limited manner to the detection of light-absorbing particles in tumors (10), to the evaluation of vascular structures (11) and blood oxygenation (12), to imaging of fluorescent proteins in model organisms (8), and to initial studies attempting to detect breast cancer in patients (13,14).

We hypothesized that MSOT could be used for real-time high-spatial-resolution imaging in cross sections through whole tumors. We investigated the ability to image dynamic contrast enhancement of tumor vasculature with use of a fluorescent dye and the visualization of targeted fluorescent probe distribution. In addition, we investigated the accumulation over time of long-circulating gold nanorods as well as intratumoral patterns of hemoglobin oxygenation to demonstrate imaging of the enhanced permeability and retention effect (15), which provides an opportunity for selective drug delivery to tumors. We performed this study to investigate whether MSOT could reveal heterogeneous distributions of exogenous agents of interest and vascular characteristics through tumors of several millimeters in diameter in vivo.

Advance in Knowledge

- It is possible, with use of multispectral optoacoustic tomography, to specifically image optical contrast—including hemoglobin oxygenation, fluorescent dyes, and light-absorbing nanoparticles—with the resolution of ultrasonography and in real time through entire tumor volumes.

Materials and Methods

MSOT Setup

The experimental MSOT system we used (Fig 1) (6,11) is capable of acquiring, reconstructing, and displaying transverse images through mice at a rate of 10 frames per second. The acquisition time was 33 μsec per frame for a 2-cm field of view; image reconstruction for the live display took less than 100 msec. The in-plane resolution was approximately 150 μm. Near-infrared excitation was provided by a tunable (700–950 nm) optical parametric oscillator pumped by an Nd:YAG laser (Opotek, Carlsbad, Calif). A fiber bundle with 10 output arms illuminated the mouse from multiple angles. A custom-made ultrasonic transducer array (Imasonic SAS, Voray, France) with 64 elements and a central frequency of 5 MHz was used for detection. The time-resolved signals were digitized by means of a custom-built acquisition system at 40 million samples per second and 12-bit digital resolution. The transducer array was submerged in a water bath for acoustic coupling to the mouse, which was placed in a horizontal position in a holder with a thin polyethylene membrane so that there was no direct contact with the water. The mouse could be translated by using a linear stage to image multiple transverse sections.

Image Reconstruction

We reconstructed the MSOT images for each wavelength by using a backprojection algorithm (16). Subsequently, linear spectral unmixing was applied to each set of multiwavelength images to resolve signals specific to each absorber (contrast agents and hemoglobin) (8). For each pixel, the method fits (with least-squares analysis) the measured overall optoacoustic spectrum to the known absorption spectra of oxy- and deoxyhemoglobin, the spectrum of the injected agent, and a flat (constant) spectrum. Each equation used for

Published online
10.1148/radiol.11111646 **Content code:** MI

Radiology 2012; 263:461–468

Abbreviations:
ICG = indocyanine green
MSOT = multispectral optoacoustic tomography

Author contributions:
Guarantors of integrity of entire study, A.T., V.N.; study concepts/study design or data acquisition or data analysis/interpretation, all authors; manuscript drafting or manuscript revision for important intellectual content, all authors; manuscript final version approval, all authors; literature research, E.H., A.T., N.B., D.R.; experimental studies, E.H., A.T., N.B., A.A.L., V.N.; statistical analysis; and manuscript editing, E.H., A.T., A.A.L., D.R., V.N.

Potential conflicts of interest are listed at the end of this article.

spectral unmixing was of the following form:

$$\phi\mu_a(\lambda_i) = \phi\sum_{j=1}^{N}\varepsilon(\lambda_i)c_j,$$

where φ is the fluence (in joules per square centimeter), μ_a the optical absorption coefficient (per centimeter), λ_i the wavelength, ε_j the wavelength-dependent absorption coefficient per concentration for the absorber j, and c_j the local concentration of that absorber. The product $\varphi\mu_a$ represents the pixel intensity at each wavelength because the optoacoustic signal amplitude is proportional to the local fluence and absorption properties. The unknown quantities solved for with least-squares analysis are then φc_j for $j = 1\ldots N$. We assume that the wavelength dependence of the fluence owing to the absorption spectrum of tissue can be neglected, a reasonable assumption in the case of subcutaneous tumors. Correction approaches for imaging in deeper tissues are a subject of current research (17).

Animal Handling

Procedures involving animals were approved by the government of Upper Bavaria. Three cancer cell lines were used: 4T1 mouse mammary tumor cells (CRL-2539; American Type Cell Culture Collection, Manassas, Va), A2780 human ovarian cancer cells (Sigma-Aldrich, St Louis, Mo), and HT29 human colon adenocarcinoma cells (ATCC-HTB-38, American Type Cell Culture Collection). The mice (adult female CD-1 nude mice) were inoculated subcutaneously with the cell suspensions (4T1 and A2780: 0.8 million cells; HT29: 1.5 million cells), and terminal experiments were performed when the tumors reached an approximate diameter of 8 mm (to have comparable dimensions). MSOT data were recorded with the mice under isofluorane anesthesia.

Dynamic Contrast Enhancement of Tumor Vasculature

To study MSOT imaging of dynamic contrast enhancement, we used indocyanine green (ICG) (Pulsion Medical Systems, Munich, Germany), a dye approved by the U.S. Food and Drug Administration with an established clinical use (18). After intravenous injection, ICG rapidly binds to plasma albumin and b-lipoproteins and leaves the circulation (19). Imaging was performed in three mice with 4T1 tumors. MSOT through the tumor was performed before and immediately, 20 minutes, 4 hours, and 24 hours after injection of 97-nmol ICG at wavelengths of 725, 750, 775, 800, 825, and 850 nm. During intravenous injection of ICG, the mice were imaged continuously at 790 nm. For comparison purposes and to verify the presence of ICG, in vivo epifluorescence images were captured at the 24-hour time point by using a cooled charge-coupled device camera (VersArray; Roper Scientific, Trenton, NJ) and appropriate emission filters, with 750-nm laser illumination. The tumor-to-background ratio was calculated with manual segmentation of tumor and adjacent skin regions, followed by division of the mean intensity values within these regions.

Figure 1

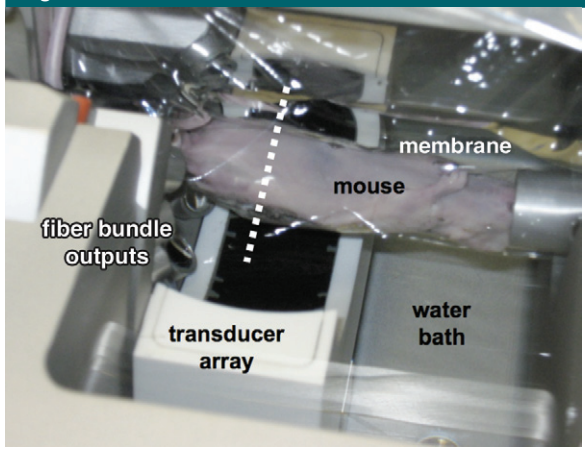

Figure 1: Experimental MSOT imaging setup. Dashed line shows approximate imaging plane.

Imaging of a Targeted Fluorescent Agent

To study the ability of MSOT to depict distributions of hemoglobin and a targeted fluorescent agent in tumors, three 4T1 tumor–bearing mice were imaged at wavelengths of 700, 730, 745, 760, 800, and 900 nm. To examine hemoglobin distributions (and therefore functional characteristics of the tumor vasculature) before injection of the targeted fluorescent agent, mice were imaged 4, 6, 10, and 13 days after tumor cell inoculation. On day 13, 24 nmol of a targeted fluorescent agent (IntegriSense 750; PerkinElmer, Waltham, Mass) was injected and imaging was performed after 6 hours. IntegriSense 750 is a 3-aminomethyl analog conjugated to a fluorescent dye that targets integrin $\alpha_v\beta_3$, a biomarker associated with disease-related angiogenesis (20,21). After MSOT, the mice were euthanized, frozen at −80°C in an optimal cutting temperature compound (Sakura Finetek, Torrance, Calif), sliced in a cryotome (CM 1950; Leica Microsystems, Wetzlar, Germany), and simultaneously imaged with a multispectral fluorescence system (22) to validate the distribution of IntegriSense 750. Images were recorded from transverse sections of the tumor at 500-μm intervals. We quantified the percentage of pixels that produced no significant oxyhemoglobin signal in MSOT sections through the tumors by means of manual segmentation of the tumor region and subsequent counting of pixels where the contribution from oxyhemoglobin was not above zero.

Imaging the Accumulation of Nanoparticles

Gold nanorods (AuNR-M; Nanopartz, Loveland, Colo) with an optical absorption peak around 780 nm were used to image accumulation by means of the enhanced permeability and retention effect, whereby the particles leak out of the defective tumor vasculature.

Figure 2

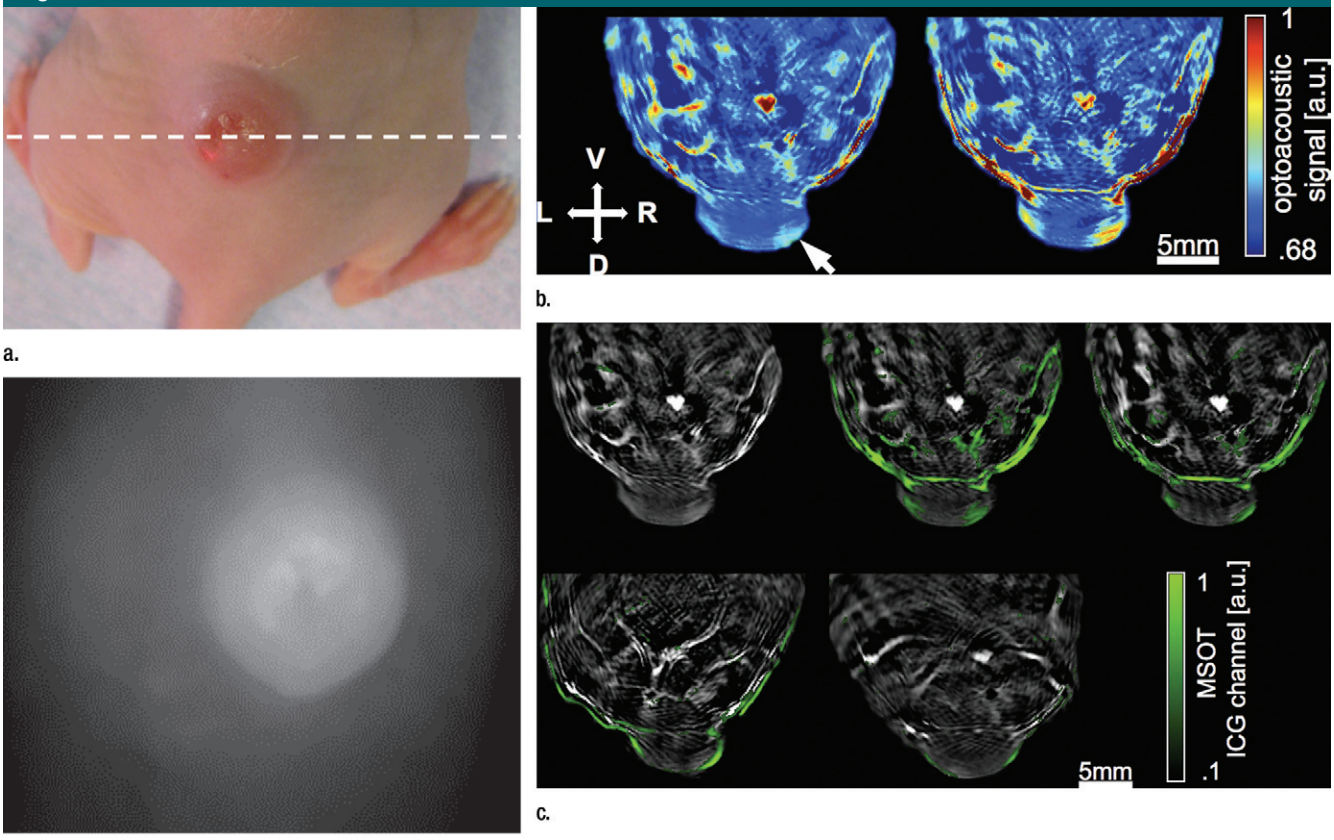

Figure 2: Dynamic contrast enhancement in nude mouse with 4T1 tumor. **(a)** Photograph of mouse with tumor; dashed line indicates imaging section. **(b)** Single-pulse images obtained at 790 nm before (left) and approximately 30 seconds after (right) ICG injection. Note the increase in contrast in and around the tumor (arrow) after injection. Further frames during injection can be seen in the supporting Movie (online). **(c)** MSOT images obtained (from top left to bottom right) before and immediately, 20 minutes, 4 hours, and 24 hours after injection of ICG. Multispectrally resolved ICG signals are overlaid in green. **(d)** Epifluorescence image obtained 24 hours after injection shows signal from ICG in tumor.

Gold nanorods display a high, tunable absorption peak in the near-infrared region. Their intense photothermal properties can be used for therapeutic purposes (23) and allow for light-mediated drug release (24). Because of their strong optical absorption, they are suitable contrast agents for optoacoustic imaging (25,26). We used nanorods coated in a proprietary layer of hydrophilic methyl-polymers, which give the particles ultralong circulation times in vivo. Their dimensions were 10×38 nm.

In initial experiments, four 4T1 tumor–bearing mice were imaged at wavelengths of 700, 730, 760, 780, 800, 825, 850, and 900 nm. Gold nanorods (16 μg/g, approximately 2.6E12 particles) were injected. Imaging was performed before injection and immediately, 1 hour, 5 hours, and 24 hours after injection. Thereafter, the mice were euthanized and blood samples obtained to check for circulating gold nanorods. After centrifugation (2000 g for 6 minutes), plasma supernatant was removed and its absorbance spectrum recorded by using a spectrometer (VIS-NIR; Ocean Optics, Dunedin, Fla). An absorption peak near 780 nm is indicative of a substantial concentration of gold nanorods. The mice were then stored at −80°C until sliced in a cryotome. Selected representative fresh-frozen 18-μm-thick slices through the tumors were collected and stained with hematoxylin-eosin. To confirm the distribution of gold nanorods, selected fresh-frozen tissue slices (10 or 12 μm) through the tumors were characterized by using an upright dark-field microscope (Axiotech; Carl Zeiss, Oberkochen, Germany). A dark-field condenser (numerical aperture = 1.2–1.4) focused white light from a halogen lamp onto the tissue. The tissue was immersed in standard index matching liquid (refractive index, 1.52) between the substrate and the condenser to reduce light scattering from the tissue background. Scattered light was collected with an objective lens (original magnification, ×100; numeric aperture = 1.0; water), and images were recorded with a charge-coupled device camera (model 550D; Canon, Newport News, Va).

In subsequent experiments, three mice with HT29 tumors and two with A2780 tumors were injected with 8 μg/g gold nanorods and imaged with MSOT at the same wavelengths and time points as in the initial study. We quantified the percentage of pixels that displayed increased gold nanorod signal in MSOT sections through the tumors by means of manual segmentation of the tumor region and subsequent comparison of each pixel with the maximum baseline level (noise) from equivalent images before agent injection.

Results

Dynamic Contrast Enhancement of Tumor Vasculature

Images obtained at 790 nm during ICG injection (Fig 2b, Movie [online]) showed a dynamic signal increase in regions inside and around the tumor. This immediate contrast enhancement arises from circulating ICG and therefore corresponds to the tumor vasculature and blood vessels elsewhere in the mouse. Specific multispectral detection of the dye was also possible (Fig 2c, green overlay). The spectrally resolved signal from ICG directly after injection (Fig 2c) corresponded well to areas of increased contrast on the live images (Fig 2b), serving as additional validation. In measurements obtained 20 minutes, 4 hours, and 24 hours after the injection (Fig 2c), we observed a rapid decrease in ICG signal as the dye disappeared from the circulation (a circulation half-life in single minutes is expected [27]) and left behind small accumulations in surrounding tissue.

On an epifluorescence image of the tumor obtained at the 24-hour time point (Fig 2d), we observed weak contrast between the tumor and surrounding tissue (tumor-to-background ratio, 1.7:1), as seen with MSOT at the same time point.

Imaging of a Targeted Fluorescent Agent

MSOT was further used to visualize a targeted fluorescent agent within tumors. With use of MSOT it was possible to identify the biodistribution of the probe 6 hours after injection (Fig 3a, validated with epifluorescence of cryosections), showing that it did not uniformly penetrate the tumor mass but was concentrated in the periphery of the tumor. From the same MSOT data, we resolved the contributions from oxygenated (red) and deoxygenated (blue) hemoglobin within the tumor (Fig 3b). This provides a possible explanation for the absence of the probe inside the tumor: 52% (2472 of 4705 pixels) of the tumor area produced no detectable oxyhemoglobin signals, indicating a lack of viable vasculature required for probe delivery. Measurements of the same tumor from 6 days after cancer cell inoculation already showed a region of concentrated deoxyhemoglobin in the tumor core (Fig 3b).

Figure 3

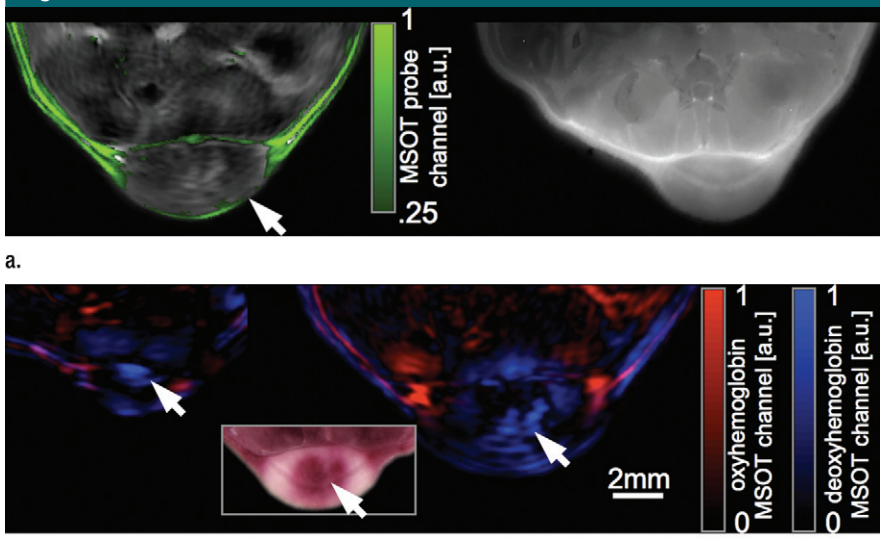

Figure 3: MSOT of hemoglobin and $\alpha_v\beta_3$-targeting fluorescent agent (IntegriSense 750) in nude mouse with 4T1 tumor. **(a)** MSOT image obtained after 6 hours of incubation (left) shows multispectrally resolved fluorescent agent signals (green overlay, arrow indicates tumor). Fluorescence image of corresponding cryosection (right) was obtained for validation. **(b)** Multispectrally resolved oxyhemoglobin (red) and deoxyhemoglobin (blue) distribution within the tumor on days 6 (left) and 13 (right). Inset is photograph of corresponding cryosection through tumor. Arrows indicate regions of deoxygenated hemoglobin in tumor core.

Imaging the Accumulation of Nanoparticles in Vivo

The initial results from long-circulating gold nanorods showed accumulation in tumors that could be detected with MSOT after 24 hours (Fig 4a). The blood plasma spectrum (Fig 4a) displayed a peak near 780 nm, confirming the presence of circulating gold nanorods 24 hours after injection. This, together with the suitable size of the nanoparticles (15), helps explain the accumulation: There is a long period during which extravasation and accumulation in the tumor by the enhanced permeability and retention effect can occur. The high spatial resolution of MSOT shows that the signal localized to parts of the tumor that showed elevated contrast on single-wavelength optoacoustic images even before the agent was injected. This suggests that agent accumulation is co-localized to contrast-producing areas of accumulated blood. As can be seen in Figure 4b, cryosection analysis helped confirm the accumulation of blood at the interface between the tumor and the surrounding tissue as well as in central tumor regions. The hematoxylin-eosin–stained images (Fig 4c) showed acellular regions at tumor margins and within the tumor nodule, where blood can accumulate. At dark-field microscopy, single nanorods and agglomerations thereof were seen as bright green, yellow, and orange because of their scattering (28). Gold nanorods were found to be sparsely

Figure 4

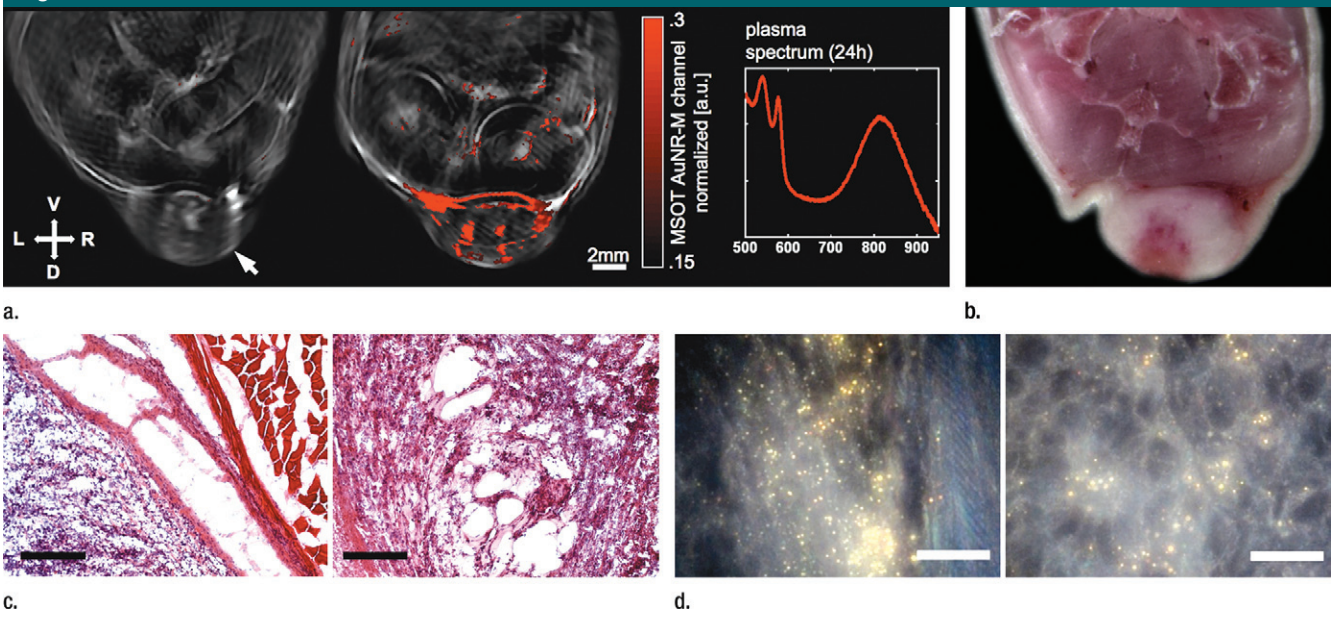

Figure 4: Gold nanorod accumulation in a nude mouse with 4T1 tumor. **(a)** Images obtained before injection (left) and 24 hours after injection (middle); multispectrally resolved gold nanorod signals are overlaid in red. Arrow indicates tumor. Graph (right) shows absorption spectrum of blood plasma 24 hours after injection, displaying the characteristic peak of gold nanorods. **(b)** Photograph of corresponding cryosection through tumor. **(c)** Photomicrographs of specimen from 4T1 tumor. Acellular regions are seen at tumor margins (left) and within tumor core (right). Scale bars = 500 μm. (Hematoxylin-eosin stain; original magnification, ×10.) **(d)** Dark-field scattering images show accumulation of gold nanorods (orange spots) along the interface between tumor and surrounding tissue (left) and within central tumor regions (right). Scale bars = 20 μm. (Original magnification, ×100.)

distributed over the tumor area (Fig 4d); however, only a few spots were found in the healthy tissue. The highest concentration of gold nanorods was detected along the interface between tumor and surrounding tissue, confirming the results obtained with MSOT.

By inspecting images of gold nanorod distribution over multiple time points (Fig 5a), we observed a changing pattern: Initially, gold nanorods were mainly found in the circulation. Images obtained 5 and 24 hours after injection showed accumulation outside of blood vessels. We characterized the percentage of tumor tissue displaying increased gold nanorod signals in two single tumors of the A2780 and HT29 cell lines. The A2780 tumor showed accumulation in a higher percentage of the measured tumor tissue (Fig 5b). Again, from the same MSOT data, we produced quantitative maps of contributions from oxy- and deoxyhemoglobin in the tumors (Fig 5c). The resulting images showed functionally differing tumor vasculatures: At inspection, the A2780 tumor had more areas of concentrated deoxygenated hemoglobin (blue) than the HT29 tumor, which, in turn, showed a more uniform distribution of oxyhemoglobin (red). These results suggest a possible relationship between the accumulation metrics and vascular architecture. Ex vivo images of cryosections obtained after the experiments agree with these in vivo results: The A2780 tumor had visible accumulations of blood in areas showing deoxyhemoglobin signal on the in vivo image (Fig 5c).

Discussion

It is possible, with use of MSOT, to specifically image optical contrast, including hemoglobin oxygenation, fluorescent dyes, and light-absorbing nanoparticles, with the resolution of ultrasonography (US) and in real time through entire tumor volumes. We saw varying patterns on our images, with a typical example being peripheral distribution around a tumor and an inability to penetrate uniformly through the tumor bulk. This detailed information about intratumoral parameters is available to MSOT because it is a high-spatial-resolution method that further displays an appropriate sensitivity for detecting molecular agents. There was a remarkable difference in appearance between the MSOT images and the epifluorescence images in this study. The latter, a typical means of understanding fluorescence agent biodistribution, offers a misleading impression of homogeneous distribution in tumors. Conversely, MSOT reveals a picture of biodistribution that reflects tumor heterogeneity.

Many of the studies were performed in live (real-time) imaging mode, requiring less than 50 μsec of acquisition time per frame. Real-time imaging, which is typical of US, can become important in dynamic clinical MSOT as well. Because of the relatively high spatial resolution, we could visualize large individual blood vessels—in particular those feeding the tumor. The resolution in optoacoustics is scalable with depth and can improve

Figure 5

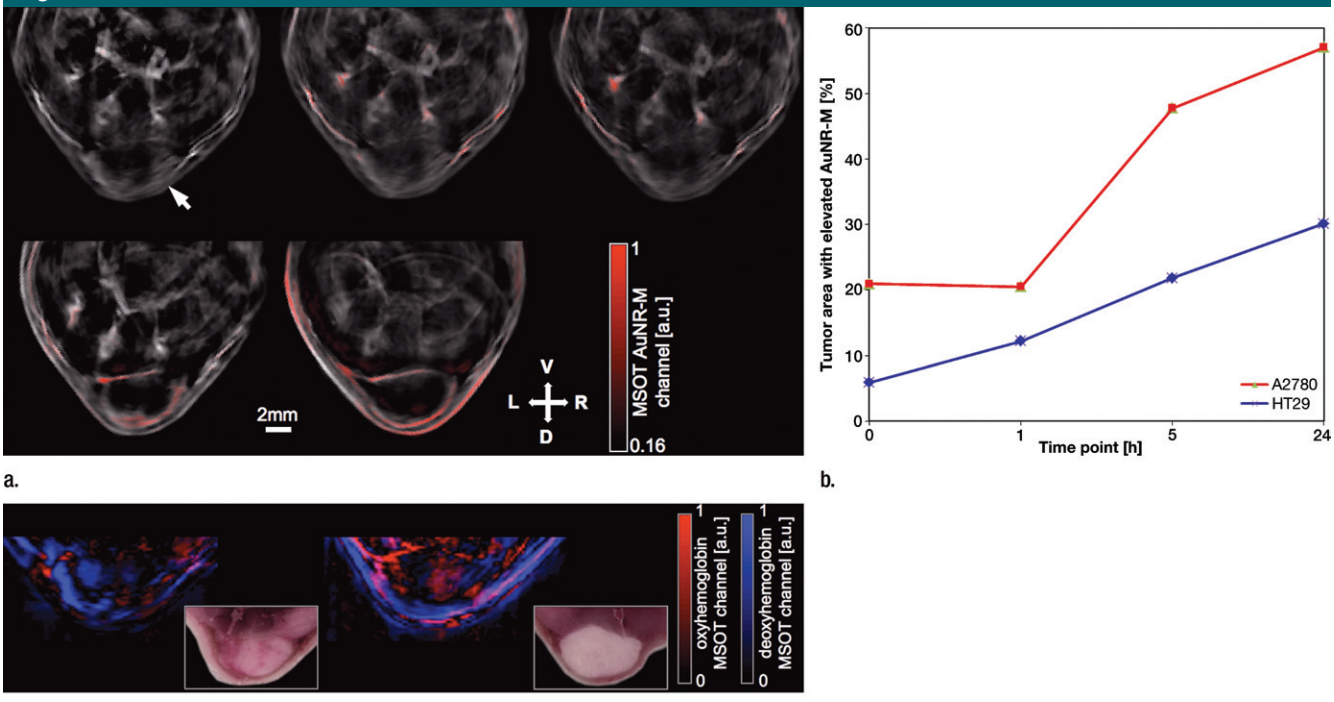

Figure 5: Gold nanorod accumulation in nude mouse with A2780 tumor. **(a)** MSOT images of multispectrally resolved gold nanorod signals (overlaid in red); images were obtained (from top left to bottom right) before and immediately, 1, 5, and 24 hours after injection. Arrow indicates tumor. **(b)** Graph shows percentage of tumor area with elevated levels of gold nanorods for two tumors of different cell lines (A2780 and HT29). **(c)** MSOT images of oxyhemoglobin (red) and deoxyhemoglobin (blue) distribution in A2780 (left) and HT29 (right) tumors reveal different vasculature. Insets are photographs of corresponding cryosections.

in the current implementation with use of higher frequency detectors. The resolution in our implementation (~150 μm, characterization not shown) was selected to allow visualization of a large field of view (~2 cm) for whole-mouse imaging.

In addition to demonstrating the spatial and temporal features of the method, we also showed that specific absorbers can be revealed by their spectral signatures, allowing imaging of an absorber of interest without the need for baseline measurements. This is particularly useful for studies in which it is necessary to obtain measurements over several hours or days. In this way, we were able to characterize the distribution of imaging agents over time. Importantly, the current MSOT implementation enables fast wavelength scans, allowing the identification of multiple spectral signatures in the same imaging section. This allowed the simultaneous imaging of oxy- and deoxyhemoglobin and an injected agent in tumors. Multiplexing additional agents should be possible provided their absorption spectra are distinct, that is, they display absorption peaks at different wavelengths. Performing studies with multiple exogenous agents simultaneously will be a subject of further investigations.

Perhaps the most important limitation of MSOT relates to its use of light, which limits the penetration depth in tissue. Typical penetration depths range from several millimeters to a few centimeters, depending on the tissue type. In the current implementation, a superficial tumor model was used for simplicity; however, anatomic features at greater depths are also visible on the images. It might therefore be possible to image orthotopic tumors, and this is proposed in future investigations. The sensitivity in detecting tumor biomarkers will, however, decrease with depth because light attenuates by approximately one to two orders of magnitude per centimeter of propagation. An additional limitation of the current system is that real-time imaging can be achieved only on a single section at a time. Therefore, although the entire tumor can be scanned sequentially, real-time imaging can be performed only on two-dimensional sections. Future developments foresee a larger detector array that can capture three-dimensional data from the entire tumor in real time.

Overall, MSOT can combine the functional and molecular ability of optical methods with the resolution of US or magnetic resonance imaging. MSOT can function as an extension of intravital microscopy: By sacrificing optical diffraction–limited resolution, one can achieve significantly larger penetration depths in tumors with the resolution of US. For many light-absorbing agents, the same contrast can then be

visualized macroscopically and microscopically. This approach could also be suitable for several applications in clinical settings—in particular in relation to handheld and endoscopic systems—thus expanding the capabilities of current clinical optical imaging.

Disclosures of Potential Conflicts of Interest: E.H. No potential conflicts of interest to disclose. **A.T.** No potential conflicts of interest to disclose. **N.B.** No potential conflicts of interest to disclose. **A.A.L.** No potential conflicts of interest to disclose. **D.R.** No potential conflicts of interest to disclose. **V.N.** Financial activities related to the present article: none to disclose. Financial activities not related to the present article: institution receives money for patents on MSOT; institution has stock or stock options in Ithera Medical. Other relationships: none to disclose.

References

1. Condeelis J, Segall JE. Intravital imaging of cell movement in tumours. Nat Rev Cancer 2003;3(12):921–930.
2. Jain RK, Munn LL, Fukumura D. Dissecting tumour pathophysiology using intravital microscopy. Nat Rev Cancer 2002;2(4):266–276.
3. Ntziachristos V. Going deeper than microscopy: the optical imaging frontier in biology. Nat Methods 2010;7(8):603–614.
4. Ntziachristos V, Razansky D. Molecular imaging by means of multispectral optoacoustic tomography (MSOT). Chem Rev 2010;110(5):2783–2794.
5. Wang LV. Multiscale photoacoustic microscopy and computed tomography. Nat Photonics 2009;3(9):503–509.
6. Buehler A, Herzog E, Razansky D, Ntziachristos V. Video rate optoacoustic tomography of mouse kidney perfusion. Opt Lett 2010;35(14):2475–2477.
7. Oraevsky AA, Jacques SL, Tittel FK. Measurement of tissue optical properties by time-resolved detection of laser-induced transient stress. Appl Opt 1997;36(1):402–415.
8. Razansky D, Distel M, Vinegoni C, et al. Multispectral opto-acoustic tomography of deep-seated fluorescent proteins in vivo. Nat Photonics 2009;3:412–417.
9. Li ML, Oh JT, Xie X, et al. Simultaneous molecular and hypoxia imaging of brain tumors in vivo using spectroscopic photoacoustic tomography. Proc IEEE 2008;96(3):481–489.
10. De la Zerda A, Zavaleta C, Keren S, et al. Carbon nanotubes as photoacoustic molecular imaging agents in living mice. Nat Nanotechnol 2008;3(9):557–562.
11. Taruttis A, Herzog E, Razansky D, Ntziachristos V. Real-time imaging of cardiovascular dynamics and circulating gold nanorods with multispectral optoacoustic tomography. Opt Express 2010;18(19):19592–19602.
12. Zhang HF, Maslov K, Sivaramakrishnan M, Stoica G, Wang LV. Imaging of hemoglobin oxygen saturation variations in single vessels in vivo using photoacoustic microscopy. Appl Phys Lett 2007;90(5):053901.
13. Ermilov SA, Khamapirad T, Conjusteau A, et al. Laser optoacoustic imaging system for detection of breast cancer. J Biomed Opt 2009;14(2):024007.
14. Manohar S, Vaartjes SE, van Hespen JCG, et al. Initial results of in vivo non-invasive cancer imaging in the human breast using near-infrared photoacoustics. Opt Express 2007;15(19):12277–12285.
15. Maeda H, Wu J, Sawa T, Matsumura Y, Hori K. Tumor vascular permeability and the EPR effect in macromolecular therapeutics: a review. J Control Release 2000;65(1-2):271–284.
16. Kruger RA, Kiser WL, Reinecke DR, Kruger GA, Miller KD. Thermoacoustic molecular imaging of small animals. Mol Imaging 2003;2(2):113–123.
17. Rosenthal A, Razansky D, Ntziachristos V. Quantitative optoacoustic signal extraction using sparse signal representation. IEEE Trans Med Imaging 2009;28(12):1997–2006.
18. Hunton DB, Bollman JL, Hoffman HN. Studies of hepatic function with indocyanine green. Gastroenterology 1960;39:713–724.
19. Cherrick GR, Stein SW, Leevy CM, Davidson CS. Indocyanine green: observations on its physical properties, plasma decay, and hepatic extraction. J Clin Invest 1960;39:592–600.
20. Hood JD, Cheresh DA. Role of integrins in cell invasion and migration. Nat Rev Cancer 2002;2(2):91–100.
21. Kossodo S, Pickarski M, Lin SA, et al. Dual in vivo quantification of integrin-targeted and protease-activated agents in cancer using fluorescence molecular tomography (FMT). Mol Imaging Biol 2010;12(5):488–499.
22. Sarantopoulos A, Themelis G, Ntziachristos V. Imaging the bio-distribution of fluorescent probes using multispectral epi-illumination cryoslicing imaging. Mol Imaging Biol 2011;13(5):874–885.
23. Dickerson EB, Dreaden EC, Huang X, et al. Gold nanorod assisted near-infrared plasmonic photothermal therapy (PPTT) of squamous cell carcinoma in mice. Cancer Lett 2008;269(1):57–66.
24. Skirtach AG, Dejugnat C, Braun D, et al. The role of metal nanoparticles in remote release of encapsulated materials. Nano Lett 2005;5(7):1371–1377.
25. Song KH, Kim C, Maslov K, Wang LV. Noninvasive in vivo spectroscopic nanorod-contrast photoacoustic mapping of sentinel lymph nodes. Eur J Radiol 2009;70(2):227–231.
26. Eghtedari M, Oraevsky A, Copland JA, Kotov NA, Conjusteau A, Motamedi M. High sensitivity of in vivo detection of gold nanorods using a laser optoacoustic imaging system. Nano Lett 2007;7(7):1914–1918.
27. Okabe A, Hirota M, Kimura Y, Maeda K, Ogawa M. Functional disturbance of biliary indocyanine green excretion in rat cerulein pancreatitis followed by endotoxemia: role of the prime and the second attack. JOP 2003;4(5):178–183.
28. Orendorff CJ, Sau TK, Murphy CJ. Shape-dependent plasmon-resonant gold nanoparticles. Small 2006;2(5):636–639.